PHOTONICS Research

Soliton frequency comb generation in CMOS-compatible silicon nitride microresonators

Yaozu Xie,[1] Jiaqi Li,[1] Yanfeng Zhang,[1,2] Zeru Wu,[1] Shihao Zeng,[1] Shuqing Lin,[1] Zhaoyang Wu,[1] Wenchao Zhou,[1] Yujie Chen,[1] and Siyuan Yu[1,3]

[1]State Key Laboratory of Optoelectronic Materials and Technologies, School of Electronics and Information Technology, Sun Yat-sen University, Guangzhou 510275, China
[2]e-mail: zhangyf33@mail.sysu.edu.cn
[3]e-mail: yusy@mail.sysu.edu.cn

Received 27 January 2022; revised 11 March 2022; accepted 17 March 2022; posted 18 March 2022 (Doc. ID 454816); published 29 April 2022

The monolithic integration of soliton microcomb devices with active photonic components and high-frequency electronics is highly desirable for practical applications. Among many materials, silicon nitride (SiN_x) waveguide layers prepared by low-pressure chemical vapor deposition (LPCVD) have been the main platform for on-chip optical frequency comb generation. However, the high temperatures involved in LPCVD render it incompatible as a back-end process with complementary metal oxide semiconductor (CMOS) or active III-V compound semiconductor fabrication flows. We report the generation of coherent soliton frequency combs in micro-ring resonators fabricated in deuterated silicon nitride (SiN_x:D) waveguides with a loss of 0.09 dB/cm. Deposited at 270°C by an inductance-coupled plasma chemical vapor deposition (ICP-CVD) process, the material preparation and fabrication flow are fully CMOS-compatible. These results enable the integration of silicon-nitride-based optical combs and photonic integrated circuits (PICs) on prefabricated CMOS and/or III-V substrates, therefore marking a major step forward in SiN_x photonic technologies.

https://doi.org/10.1364/PRJ.454816

1. INTRODUCTION

On-chip optical frequency combs could revolutionize a vast range of applications such as optical atomic clocks [1], astronomy [2,3], coherent optical communication [4,5], ultrafast distance measurements by means of LIDAR [6–9], spectroscopy [10], and integrated microwave photonics [11,12]. It could also be applied in optical neural computing [13,14] and quantum optics [15,16]. Silicon nitride (SiN_x) has been the main platform for optical comb generation by way of Kerr nonlinearity as the material combines the lowest linear loss with a relatively high refractive index and strong Kerr effect among many material platforms [17]. SiN_x is widely used in microelectronic and photonic fabrication flows, making it a readily acceptable candidate for monolithic integration with active photonic components and high-frequency electronics, which would be key to the practical applications of optical comb sources.

A summary of progress in SiN_x waveguide loss and Kerr nonlinear optical combs is provided in Fig. 1. The majority of the reported SiN_x photonic devices, and all of those used for soliton comb generation, have been fabricated in SiN_x materials prepared via low-pressure chemical vapor deposition (LPCVD) at around 700°C–800°C and annealed at >1000°C. LPCVD SiN_x has excellent qualities including low optical loss and high density that make it very well suited for Kerr optical comb generation. However, the high deposition and annealing temperatures will destroy any front-end-of-the-line (FEOL) silicon or III-V compound semiconductor components that need to be integrated with the SiN_x photonic circuits. Therefore, LPCVD SiN_x as a back-end process is incompatible with complementary metal oxide semiconductor (CMOS) or III-V electronic and/or photonic circuitry prefabricated on the same wafer. Although heterogeneously integrated laser soliton microcombs have been demonstrated recently [24], it could only be achieved through post-process methods such as chemical-mechanical polishing (CMP) and wafer bonding.

As an alternative, low-temperature (<400°C) SiN_x deposition processes including plasma enhanced chemical vapor deposition (PECVD) [22,25], sputtering [26], or other annealing-free processes [27] have been investigated. These processes have the potential of integrating SiN_x photonic layers on top of prefabricated electronic or active optoelectronic layers. Additional advantages include easier strain management, which is crucial for depositing thick waveguide layers often required by nonlinear devices due to waveguide dispersion tailoring.

Several groups invested much effort in reducing the propagation loss of low-temperature SiN_x platforms so that high

quality (Q) factor micro-cavities necessary for efficient soliton formation can be fabricated, as summarized in Fig. 1. In the absence of high-temperature annealing that expels remnant hydrogen (H) ions from conventional silane (SiH_4) source gas, an important approach is to use deuterated silane (SiD_4) as the Si source gas [22,25,28]. This removes the absorption peak at ~1520 nm caused by the remnant Si–H bonds, resulting in deuterated silicon nitride (SiN_x:D) materials that enable low loss waveguides to be fabricated across the entire telecommunications wavelength window [29]. As reported waveguide loss steadily reduced, the resulting increase in micro-cavity Q values enabled nonlinear processes to emerge. Noisy modulation instability (MI) combs have been reported in the PECVD SiN_x:D micro-ring cavity featuring a waveguide loss of 0.3–0.5 dB/cm [22,30]. The low loss SiN_x:D material platform also exhibited its potential of direct hybrid integration in integrated photonic circuits including arrayed-waveguide gratings [28], microwave photonic filters [31], modulators [32], and division-multiplexing transmitters [33].

In addition to the removal of the hydrogen bond, a key factor in improving the quality of the SiN_x:D films is to increase its density as well as to reduce granularity and formation of clusters. While the widely used capacitance-coupled PECVD technique tends to produce SiN_x films of relatively low density, high density plasma processes offer advantages in these aspects of material characteristics. By means of an inductance-coupled plasma chemical vapor deposition (ICP-CVD) process, our group has been able to steadily refine the quality of the SiN_x:D material [25,34,35], culminating in the generation of low-noise soliton crystal frequency combs in SiN_x:D micro-ring resonators (MRRs) with waveguide loss as low as 0.17 dB/cm [23]. But the single soliton state that simultaneously possesses low noise, high coherence, and single free spectral region (FSR) spectrum with a smooth envelope has so far been elusive in devices fabricated in low-temperature SiN_x waveguides due to strong thermal nonlinear effects associated with relatively higher absorption loss and lower density compared to LPCVD SiN_x.

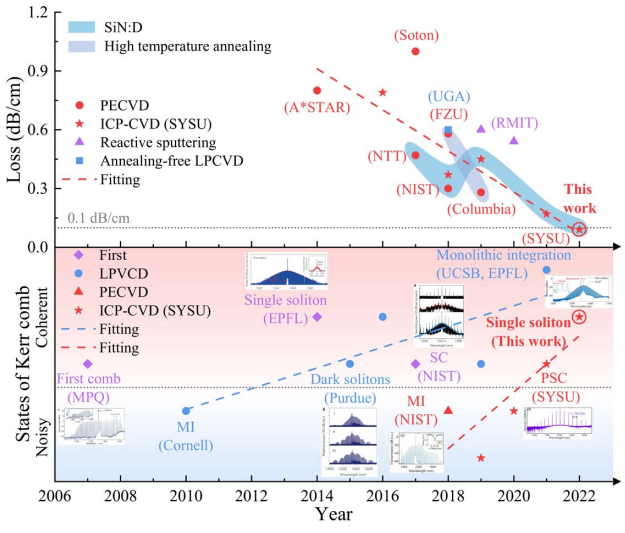

Fig. 1. Overview of the propagation loss in low-temperature SiN_x waveguides (upper panel) where the gray dashed line indicates the value of 0.1 dB/cm, while states of Kerr combs based on both LPCVD and other SiN_x platforms are shown in the lower panel where the gray dashed line separates the effective blue/red-detuning regions corresponding to the noisy/coherent Kerr combs. MI, modulation instability; SC, soliton crystal; PSC, perfect soliton crystal. All used images are taken from Refs. [18–23].

In this paper, we report the first-known experimental generation of such soliton frequency combs in a high-Q MRR fabricated in a low-temperature SiN_x platform. Fabricated in ICP-CVD deposited SiN_x:D with a waveguide loss of 0.09 dB/cm, various soliton microcomb devices with repetition rates of 50–240 GHz are manufactured on a single substrate and successfully demonstrate low noise and coherent soliton frequency comb generation, verifying the viability of the low-temperature ICP-CVD SiN_x:D platform for integrated nonlinear photonics.

2. CHARACTERISTICS OF THE LOW-TEMPERATURE ICP-CVD SiN_x WAVEGUIDE

All SiN_x:D MRR devices are fabricated as described in Section 4.A. A device with a radius of 480 μm and a waveguide cross section of 2.2 μm × 0.85 μm (width × height) is used to characterize the waveguide quality. This relatively large device is used in order to characterize waveguide loss with minimal contribution from bending loss. The height of 0.85 μm is designed for dispersion management purposes as described later. The width of the bus waveguide is designed to be 1.5 μm for efficient excitation of the fundamental transverse mode in the MRR waveguide. A fixed gap of 275 nm between the MRR and the bus waveguide makes the MRR slightly undercoupled with a coupling rate $\kappa_{ex}/2\pi$ of 3.15×10^7 s^{-1}. These parameters allow the derivation of waveguide loss from the measured intrinsic Q-factor (Q_i) of the MRR. As shown in Fig. 2(a), this device exhibits measured Q_i of up to 5.3 million at 1561.864 nm, corresponding to a derived propagation loss value of 0.06 dB/cm.

The dependence of propagation loss on the wavelength shown in Fig. 2(b) is obtained by fitting 454 fundamental transverse electric (TE_0) resonances respectively [as plotted in Fig. 2(a)] throughout the 1465–1645 nm wavelength range. In the 1545–1625 nm wavelength range [outside the spectral range where cladding hydrogen absorption is visible as shown in Fig. 2(b)], the most probable value of waveguide loss is 0.09 dB/cm, as seen in the histogram of Fig. 2(c). This is the first reported waveguide loss of <0.1 dB/cm in low-temperature SiN_x, with almost all other ultralow loss (<0.1 dB/cm at 1550 nm) results achieved in LPCVD SiN_x with high-temperature thermal annealing (above 1200°C) [17,36–44]. The propagation loss in the entire 1465–1645 nm wavelength range in Fig. 2(d) has a higher most probable value of 0.12 dB/cm, mainly because at around 1515 nm (the N–H bond absorption peak) the loss value is ~0.07 dB above the mean value (the dashed line), which is attributed to the H-content in the silica upper-cladding, which is deposited using silane source (SiO_x:H) [23]. The loss of the platform could, therefore, be further reduced by utilizing hydrogen-free deuterated silica (SiO_x:D) material [45]. Combined with minimized scattering loss by means of the optimized fabrication process including CMP and photoresist reflow [42,46], low temperature deposited

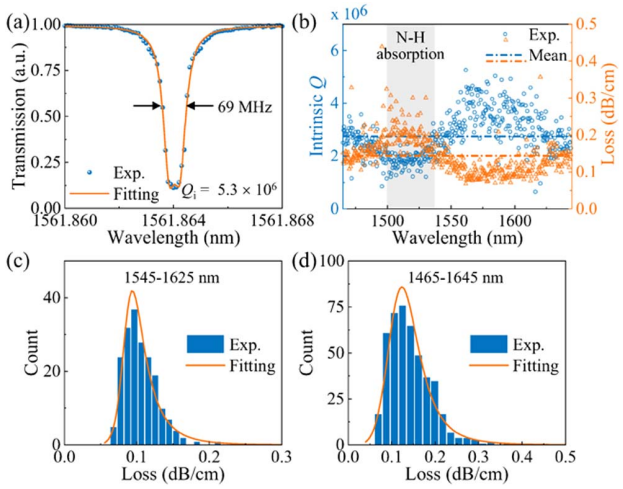

Fig. 2. (a) Measured and fitted TE_0 resonance at 1561.864 nm from the 480 μm radius SiN_x:D MRR. (b) Measured Q_i and propagation loss of the MRR. Mean values (dashed line) are shown for reference. The gray area indicates the wavelength range of N–H bond absorption due to the SiO_x:H cladding. (c) Histogram and burr fitting of propagation loss in the 1545–1625 nm wavelength range over 194 TE_0 resonances. (d) Histogram and burr fitting of propagation loss in the 1465–1645 nm wavelength range over 454 TE_0 resonances.

SiN_x:D waveguides with ultralow loss of <0.1 dB/cm across the entire telecommunications band should be achievable.

3. GENERATION OF SOLITON FREQUENCY COMBS

A 160-μm-radius MRR shown in Fig. 3(a) with the same waveguide cross section and bus waveguide coupling as the previous device is selected to conduct the Kerr frequency comb experiment. The measured FSR is around 150 GHz, and fiber-chip coupling loss is 2.35 dB per facet with the use of inverse taper mode expanders at either end of the bus waveguide. As shown in Fig. 3(b), resonances of the TE_0 mode within the 1500–1600 nm wavelength range have high extinction ratio and negligible higher-order modes. With the mean loaded Q (Q_L) being 1.3×10^6, the extracted mean Q_i is 2×10^6. The resonance at ∼1560.39 nm with a higher Q_L of 1.5×10^6 shown in Fig. 3(c) is used as the pump mode because threshold power for parametric oscillation is inversely proportional to Q_L^2. Finite element (FE) simulation shows that the MRR waveguide has anomalous dispersion with the group velocity dispersion given by $D_2/2\pi = 0.89$ MHz at 192.3 THz, meeting the phase-matching requirement of parametric conversion in four-wave mixing.

In order to readily access and study dissipative Kerr solitons (DKSs) in the SiN_x:D MRRs via slow pump laser tuning, heating with an auxiliary laser is used to mitigate the thermo-optical effects [47]. The auxiliary mode intentionally uses a TM_0 resonance at 1546.047 nm with relatively low Q_L of 0.50×10^6 and Q_i of 0.65×10^6 to avoid the noise resulting from the incoherent heterodyne beating between the backscattered auxiliary laser and the comb line in the same resonance [48] or the superposition of the backscattered noisy comb generated by the auxiliary mode on the output soliton combs. For our devices, TM_0 modes with lower Q_i naturally become a more suitable choice as the auxiliary modes, providing sufficient thermal compensation due to larger absorption loss compared with TE_0 resonances while preventing the entry of the MI state.

The high Q and low loss SiN_x:D MRR offers a threshold power of 23.7 mW (all power values are on-chip) to observe optical parametric oscillation with the first pairs of sidebands. With the pump laser power increased to 130 mW, a noisy MI comb emerges, providing a prerequisite for the formation of soliton states. Then the power and wavelength λ_{Aux} of the auxiliary laser are tuned carefully to mitigate the thermal effect according to the nonlinear response of comb power in the cavity with the sweeping speed of pump laser at 1 nm/s, while the auxiliary laser always remains in the blue-detuned region. When auxiliary laser power reaches 190 mW, by tuning λ_{Aux} from 1546.00 to 1546.36 nm to bring the auxiliary laser into the resonance, the nonlinear curve of comb power that had a typical triangle with a length of ∼100 ms due to the influence of thermal nonlinear effects [19] is shortened significantly to ∼3 ms, making the MRR transitions be thermally stable, as shown in Fig. 3(d). From the enlarged inset in Fig. 3(d), multiple soliton steps are clearly observed, verifying the generation and switching between different soliton states. The pump wavelength is tuned slowly and manually to access these comb states in turn. Output spectra in Fig. 3(e) exhibit several transitions successively from the primary state (I), to MI states (II, III), and soliton states (IV, V). The discrepancies between the fitted and measured results for optical spectra are mainly attributed to the spontaneous emission noise from erbium-doped fiber amplifiers (EDFAs).

The single soliton state with the repetition rate of 150 GHz is further characterized because its symmetric and smooth $sech^2$ spectral envelope is generally considered to be more valuable in practical applications than that of multi-soliton states. The spectrum fit shows a 3 dB bandwidth (BW) of 36 nm, corresponding to a transform-limited pulse duration of 70.7 fs. As shown in Fig. 3(f), the single soliton comb is redshifted globally for about 3.6 nm compared with the pump laser due to energy transfer of photons from high to low frequencies by Raman scattering [49]. In the MI state, the electric noise spectra in Fig. 3(g) show obvious intensity noise above the background noise floor, which abruptly vanishes as the Kerr comb goes into the single soliton state. Heterodyne beat note measurement shown in Fig. 3(h) between the selected comb line and a highly coherent laser (with a linewidth of <100 Hz) positioned at 1549.982 nm exhibits a narrow RF linewidth of ∼138 kHz, highlighting the high coherence and low noise of the soliton frequency comb.

Multiple MRR devices with different radii were fabricated on the same SiN_x:D chip, and various soliton frequency combs with repetition rates of 50–240 GHz have been obtained readily in these devices at pump power below 220 mW in the same manner as in the 150 GHz MRR, as shown in Fig. 4. Though operating with larger mode volume (larger radius) requires higher pump power to build up optical intensity in the cavity, low-repetition-rate soliton microcomb devices possess higher Q_i (Fig. 2) due to negligible bending loss; hence, only a slight increase in operating power is required. The 50 GHz

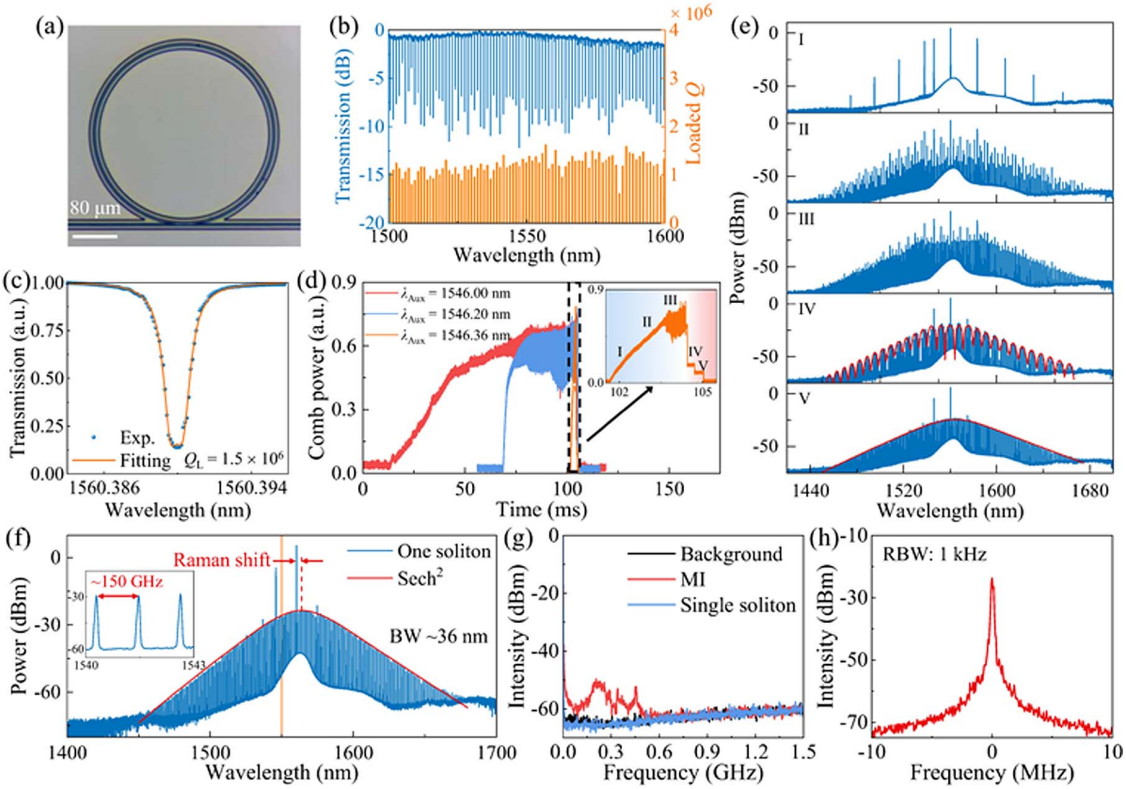

Fig. 3. (a) Micrograph of a SiN_x:D MRR with a radius of 160 μm. (b) Measured transmission spectrum and corresponding Q_L in the wavelength range of 1500–1600 nm. (c) Measured and fitted TE_0 resonance at around 1560.39 nm. (d) Measured comb power evolutions for different wavelengths of the auxiliary laser λ_{Aux} with the power of ~190 mW, as a continuous wave (CW) pump laser with the power of ~130 mW adiabatically scans from the blue- to red-detuning regimes of the pump mode at the speed of 1 nm/s. The enlarged image for the wavelength of 1546.36 nm is shown as the inset. (e) Optical spectra of the generated frequency combs referring to different pump detuning positions in (d), where fitted curves of soliton states are also presented. (f) Optical spectrum as well as its $sech^2$ fitted envelop of the single soliton state. A local oscillator laser at 1549.982 nm (the yellow solid line) for heterodyne beat note measurement is shown as a reference. The enlarged inset indicates the FSR of ~150 GHz. (g) Intensity noise spectra of the background, the MI state, and the single soliton state. (h) Beat note between the selected comb line and the local oscillating laser for the state of the single soliton. RBW, resolution bandwidth.

soliton microcomb device, due to its large dimension, is more susceptible to fabrication-induced surface roughness or imperfection. Several spectral spikes resulting from strong mode crossings between multiple optical mode families are observed clearly, which can be suppressed by optimizing coupling conditions for mode matching or utilizing a narrower ring width. Spectral BW has been measured to be in the 32–56 nm range, corresponding to soliton transform-limited pulse durations of 79.6–45.5 fs. These results cover a range of typical repetition rates for a microresonator-based frequency comb (tens of GHz to several THz), verifying the universality and maturity of our low-temperature SiN_x platform for integrated nonlinear photonics.

4. EXPERIMENTAL SECTION

A. Device Fabrication

The SiN_x:D film with the thickness of 850 nm is deposited at a temperature of 270°C on a silicon wafer with a 3 μm thermally-grown silica (SiO_2) layer, using deuterated silane (SiD_4) and pure N_2 as the source gases. The layer is deposited in one continuous run utilizing the ICP-CVD technology without high-temperature annealing and is not polished by CMP. The refractive index of the SiN_x:D film at 1550 nm is measured by ellipsometry as about 1.96, which is used for the simulation of mode profiles and dispersion. The thickness is chosen to satisfy the anomalous dispersion condition of bright solitons.

Devices in this work are fabricated solely by subtractive processing. The pattern of MRR devices is defined by means of electron beam lithography (EBL) in AR-P 6200 resist with a thickness of 800 nm and then is transferred to the SiN_x:D film by reactive ion etching (RIE) with the gases of CHF_3 and O_2. The etched waveguides, with the photoresist removed, are cladded with an ICP-CVD silica layer of 2.8 μm, which is deposited using silane (SiH_4) as the source gas. The width of the MRR waveguide is designed to be 2.2 μm and supports TE_{00}, TE_{10} modes. This width is designed to minimize optical field overlap with the etched waveguide sidewalls without having too many higher-order modes. The access bus waveguide width is a single-mode waveguide designed so that its propagation constant is synchronous with the TE_{00} mode in the MRR waveguide to enable selective excitation.

B. Device Characterization

The transmission spectra of MRRs are measured by wavelength scanning using a Keysight 8164B Lightwave Measurement

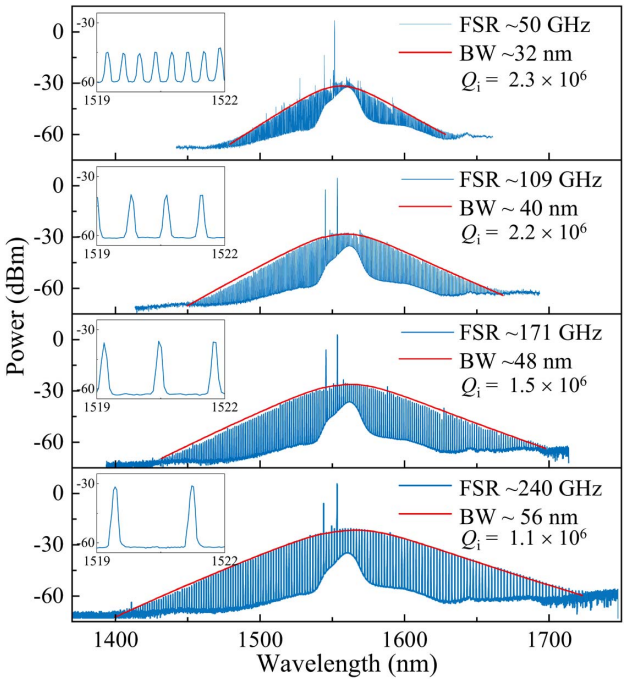

Fig. 4. Optical spectra of single soliton combs with repetition rates of 50–240 GHz generated from MRRs with different radii. The enlarged insets show the spectral details from 1519 to 1522 nm wavelength range.

System. The output from a narrow-linewidth tunable laser (Keysight 81606A TLS) is edge-coupled through a single-mode lensed fiber to the inverse-tapered SiN_x waveguides with a tip width of 200 nm. Loaded Q values obtained by fitting each resonance using a Lorentzian line shape model or a resonance doublet model [40] with excellent goodness-of-fit (GOF) statistics (>0.99) throughout the whole wavelength range are used to extract Q_i and external Q (Q_{ex}). The propagation loss values of waveguides are calculated by $2\pi n_g/(Q_i\lambda_0)$, where n_g is the group index and λ_0 is the resonant wavelength. Based on the refractive index of the SiN_x:D film fitted with the Sellmeier equation, the group velocity dispersion D_2 of MRRs is obtained by FE simulation.

C. Soliton Frequency Comb Generation Setup

An auxiliary laser is used to mitigate the thermo-optical effects to allow the robust generation of DKSs in SiN_x:D MRRs via slow laser tuning [47]. Two tunable CW lasers amplified by EDFAs are coupled into the MRRs in opposite directions. One (Toptica DLC CTL 1550) acts as the pump laser, and the other acts as the auxiliary laser (Keysight 81606A). The generated optical signal from the auxiliary end is divided into three branches for further characterizing. One branch, with the pump and auxiliary laser filtered out, is detected by a photodetector and fed into a digital oscilloscope (SIGLENT SDS6204 H12 Pro) to monitor the comb power evolution and determine whether the Kerr comb enters soliton states using the soliton steps as indicators. The second branch is connected with an optical spectrum analyzer (Anritsu MS9740A) for recording the spectra. The last branch is used to characterize the intensity noise and coherence of the Kerr comb with an electric spectrum analyzer (SIGLENT SSA3075X Plus), where the beat note between the selected comb line and a local oscillating laser (NKT Koheras ADJUSTIK E15 Power) can be analyzed.

5. CONCLUSION

By means of an optimized ICP-CVD process using deuterated silane (SiD_4) as the Si source, high density and very low loss deuterated SiN_x:D material has been deposited at 270°C with a thickness of 0.85 μm in a single step. The propagation loss of waveguides fabricated in this material averages 0.09 dB/cm in the wavelength range of 1545–1625 nm, which to the best of our knowledge is the first reported sub-0.1 dB/cm value for low-temperature SiN_x waveguides. The fabrication process is fully compatible with substrates carrying prefabricated CMOS or III-V semiconductor active components.

High Q-factor MRRs fabricated on this platform have been used to experimentally generate soliton frequency combs with repetition rates of 50–240 GHz, which to our best knowledge is the first report of soliton states, especially coherent single soliton states, with low pump power, narrow comb lines, and a wide range of repetition rates on CMOS-compatible low-temperature SiN_x platforms. These results demonstrate the viability of the low-temperature ICP-CVD SiN_x:D platform in linear as well as nonlinear integrated photonics in terms of its processing flexibility and compatibility. Such a platform is likely to have significant potentials in monolithic heterogeneous integration of passive, active, and nonlinear photonics.

Funding. National Natural Science Foundation of China (61975243); Basic and Applied Basic Research Foundation of Guangdong Province (2019A1515010858, 2021B1515020093); Science and Technology Program of Guangzhou (202103030001); Science and Technology Planning Project of Guangdong Province (2018B010114002); Local Innovative and Research Teams Project of Guangdong Pearl River Talents Program (2017BT01X121).

Disclosures. The authors declare no conflicts of interest.

Data Availability. The data that support the findings of this study are available from the corresponding author upon reasonable request.

REFERENCES

1. Z. L. Newman, V. Maurice, T. Drake, J. R. Stone, T. C. Briles, D. T. Spencer, C. Fredrick, Q. Li, D. Westly, B. R. Ilic, B. Shen, M.-G. Suh, K. Y. Yang, C. Johnson, D. M. S. Johnson, L. Hollberg, K. J. Vahala, K. Srinivasan, S. A. Diddams, J. Kitching, S. B. Papp, and M. T. Hummon, "Architecture for the photonic integration of an optical atomic clock," Optica **6**, 680–685 (2019).
2. E. Obrzud, M. Rainer, A. Harutyunyan, M. H. Anderson, J. Liu, M. Geiselmann, B. Chazelas, S. Kundermann, S. Lecomte, M. Cecconi, A. Ghedina, E. Molinari, F. Pepe, F. Wildi, F. Bouchy, T. J. Kippenberg, and T. Herr, "A microphotonic astrocomb," Nat. Photonics **13**, 31–35 (2019).
3. M. G. Suh, X. Yi, Y. H. Lai, S. Leifer, I. S. Grudinin, G. Vasisht, E. C. Martin, M. P. Fitzgerald, G. Doppmann, J. Wang, D. Mawet, S. B. Papp, S. A. Diddams, C. Beichman, and K. Vahala, "Searching for

exoplanets using a microresonator astrocomb," Nat. Photonics **13**, 25–30 (2019).
4. P. Marin-Palomo, J. N. Kemal, M. Karpov, A. Kordts, J. Pfeifle, M. H. P. Pfeiffer, P. Trocha, S. Wolf, V. Brasch, M. H. Anderson, R. Rosenberger, K. Vijayan, W. Freude, T. J. Kippenberg, and C. Koos, "Microresonator-based solitons for massively parallel coherent optical communications," Nature **546**, 274–279 (2017).
5. A. Fülöp, M. Mazur, A. Lorences-Riesgo, Ó. B. Helgason, P. H. Wang, Y. Xuan, D. E. Leaird, M. Qi, P. A. Andrekson, A. M. Weiner, and V. Torres-Company, "High-order coherent communications using mode-locked dark-pulse Kerr combs from microresonators," Nat. Commun. **9**, 1 (2018).
6. M. G. Suh and K. J. Vahala, "Soliton microcomb range measurement," Science **359**, 884–887 (2018).
7. P. Trocha, M. Karpov, D. Ganin, M. H. P. Pfeiffer, A. Kordts, S. Wolf, J. Krockenberger, P. Marin-Palomo, C. Weimann, S. Randel, W. Freude, T. J. Kippenberg, and C. Koos, "Ultrafast optical ranging using microresonator soliton frequency combs," Science **359**, 887–891 (2018).
8. J. Riemensberger, A. Lukashchuk, M. Karpov, W. Weng, E. Lucas, J. Liu, and T. J. Kippenberg, "Massively parallel coherent laser ranging using a soliton microcomb," Nature **581**, 164–170 (2020).
9. J. Wang, Z. Lu, W. Wang, F. Zhang, J. Chen, Y. Wang, J. Zheng, S. T. Chu, W. Zhao, B. E. Little, X. Qu, and W. Zhang, "Long-distance ranging with high precision using a soliton microcomb," Photon. Res. **8**, 1964–1972 (2020).
10. M. G. Suh, Q. F. Yang, K. Y. Yang, X. Yi, and K. J. Vahala, "Microresonator soliton dual-comb spectroscopy," Science **354**, 600–603 (2016).
11. W. Liang, D. Eliyahu, V. S. Ilchenko, A. A. Savchenkov, A. B. Matsko, D. Seidel, and L. Maleki, "High spectral purity Kerr frequency comb radio frequency photonic oscillator," Nat. Commun. **6**, 7957 (2015).
12. D. T. Spencer, S. H. Lee, D. Y. Oh, M.-G. Suh, K. Y. Yang, and K. Vahala, "An optical-frequency synthesizer using integrated photonics," Nature **557**, 81–85 (2018).
13. X. Xu, M. Tan, B. Corcoran, J. Wu, A. Boes, T. G. Nguyen, S. T. Chu, B. E. Little, D. G. Hicks, R. Morandotti, A. Mitchell, and D. J. Moss, "11 TOPS photonic convolutional accelerator for optical neural networks," Nature **589**, 44–51 (2021).
14. J. Feldmann, N. Youngblood, M. Karpov, H. Gehring, X. Li, M. Stappers, M. Le Gallo, X. Fu, A. Lukashchuk, A. S. Raja, J. Liu, C. D. Wright, A. Sebastian, T. J. Kippenberg, W. H. P. Pernice, and H. Bhaskaran, "Parallel convolutional processing using an integrated photonic tensor core," Nature **589**, 52–58 (2021).
15. Z. Yang, M. Jahanbozorgi, D. Jeong, S. Sun, O. Pfister, H. Lee, and X. Yi, "A squeezed quantum microcomb on a chip," Nat. Commun. **12**, 1 (2021).
16. Y. Zhang, M. Menotti, K. Tan, V. D. Vaidya, D. H. Mahler, L. G. Helt, L. Zatti, M. Liscidini, B. Morrison, and Z. Vernon, "Squeezed light from a nanophotonic molecule," Nat. Commun. **12**, 8 (2021).
17. M. W. Puckett, K. Liu, N. Chauhan, Q. Zhao, N. Jin, H. Cheng, J. Wu, R. O. Behunin, P. T. Rakich, K. D. Nelson, and D. J. Blumenthal, "422 million intrinsic quality factor planar integrated all-waveguide resonator with sub-MHz linewidth," Nat. Commun. **12**, 934 (2021).
18. P. Del'Haye, A. Schliesser, O. Arcizet, T. Wilken, R. Holzwarth, and T. J. Kippenberg, "Optical frequency comb generation from a monolithic microresonator," Nature **450**, 1214–1217 (2007).
19. T. Herr, V. Brasch, J. D. Jost, C. Y. Wang, N. M. Kondratiev, M. L. Gorodetsky, and T. J. Kippenberg, "Temporal solitons in optical microresonators," Nat. Photonics **8**, 145–152 (2014).
20. X. Xue, Y. Xuan, Y. Liu, P. H. Wang, S. Chen, J. Wang, D. E. Leaird, M. Qi, and A. M. Weiner, "Mode-locked dark pulse Kerr combs in normal-dispersion microresonators," Nat. Photonics **9**, 594–600 (2015).
21. D. C. Cole, E. S. Lamb, P. Del'Haye, S. A. Diddams, and S. B. Papp, "Soliton crystals in Kerr resonators," Nat. Photonics **11**, 671–676 (2017).
22. J. Chiles, N. Nader, D. D. Hickstein, S. P. Yu, T. C. Briles, D. Carlson, H. Jung, J. M. Shainline, S. Diddams, S. B. Papp, S. W. Nam, and R. P. Mirin, "Deuterated silicon nitride photonic devices for broadband optical frequency comb generation," Opt. Lett. **43**, 1527–1530 (2018).
23. Z. Wu, Y. Zhang, S. Zeng, J. Li, Y. Xie, Y. Chen, and S. Yu, "Low-noise Kerr frequency comb generation with low temperature deuterated silicon nitride waveguides," Opt. Express **29**, 29557–29566 (2021).
24. C. Xiang, J. Liu, J. Guo, L. Chang, R. N. Wang, W. Weng, J. Peters, W. Xie, Z. Zhang, J. Riemensberger, J. Selvidge, T. J. Kippenberg, and J. E. Bowers, "Laser soliton microcombs heterogeneously integrated on silicon," Science **373**, 99–103 (2021).
25. Z. Wu, Z. Shao, Z. Xu, Y. Zhang, L. Liu, C. Yang, Y. Chen, and S. Yu, "High quality factor deuterated silicon nitride (SiN:D) microring resonators," in *Conference on Lasers and Electro-Optics/Pacific Rim* (2018), paper W4D.5.
26. A. Frigg, A. Boes, G. Ren, I. Abdo, D.-Y. Choi, S. Gees, and A. Mitchell, "Low loss CMOS-compatible silicon nitride photonics utilizing reactive sputtered thin films," Opt. Express **27**, 37795–37805 (2019).
27. H. El Dirani, A. Kamel, M. Casale, S. Kerdiles, C. Monat, X. Letartre, M. Pu, L. K. Oxenløwe, H. El Dirani, A. Kamel, M. Casale, S. Kerdiles, C. Monat, H. El Dirani, A. Kamel, M. Casale, and S. Kerdiles, "Annealing-free Si_3N_4 frequency combs for monolithic integration with Si photonics," Appl. Phys. Lett. **113**, 081102 (2018).
28. T. Hiraki, T. Aihara, H. Nishi, and T. Tsuchizawa, "Deuterated SiN/SiON waveguides on Si platform and their application to C-band WDM filters," IEEE Photon. J. **9**, 2500207 (2017).
29. A. V. Osinsky, R. A. Bellman, I. A. Akwani, P. A. Sachenik, S. L. Logunov, and J. W. McCamy, "Optical loss mechanisms in GeSiON planar waveguides," Appl. Phys. Lett. **81**, 2002–2004 (2002).
30. Z. Wu, S. Zeng, Y. Chen, Y. Zhang, and S. Yu, "Frequency comb generation in a deuterated-SiN_x micro-ring resonator with sidewall Bragg gratings," in *Frontiers in Optics* (2020), paper FW4D.2.
31. S. Tang, Y. Zhang, Z. Wu, L. Zhou, L. Liu, Y. Chen, and Y. Yu, "Tunable microwave photonic filter based on silicon nitride MZI-assist micro-ring resonator," in *Asia Communications and Photonics Conference* (2019), paper M3E.4.
32. T. Hiraki, T. Aihara, K. Takeda, T. Fujii, T. Kakitsuka, T. Tsuchizawa, H. Fukuda, and S. Matsuo, "Membrane InGaAsP Mach-Zehnder modulator with SiN:D waveguides on Si platform," Opt. Express **27**, 18612–18619 (2019).
33. H. Nishi, T. Fuji, N. P. Diamantopoulos, K. Takeda, E. Kanno, T. Kakitsuka, T. Tsuchizawa, H. Fukuda, and S. Matsuo, "Integration of eight-channel directly modulated membrane-laser array and SiN AWG multiplexer on Si," J. Lightwave Technol. **37**, 266–273 (2019).
34. Z. Wu, Z. Xu, Y. Zhang, H. Chen, Y. Chen, and S. Yu, "Four-wave mixing parametric oscillation in deuterated silicon nitride microresonators prepared by low-temperature (100 °C) PECVD platform," in *European Conference on Lasers and Electro-Optics* (2019), paper ce_4_5.
35. Z. Wu, Y. Chen, Z. Xu, L. Liu, H. Chen, Y. Zhang, and S. Yu, "Waveguide-integrated deuterated silicon nitride (SiN:D) microdisk resonators for nonlinear photonics," in *Asia Communications and Photonics Conference* (2019), pp. 1–3.
36. D. T. Spencer, J. F. Bauters, M. J. R. Heck, and J. E. Bowers, "Integrated waveguide coupled Si_3N_4 in the ultrahigh-*Q* regime," Optica **1**, 153–157 (2014).
37. W. Jin, Q. F. Yang, L. Chang, B. Shen, H. Wang, M. A. Leal, L. Wu, M. Gao, A. Feshali, M. Paniccia, K. J. Vahala, and J. E. Bowers, "Hertz-linewidth semiconductor lasers using CMOS-ready ultra-high-*Q* microresonators," Nat. Photonics **15**, 346–353 (2021).
38. K. Luke, A. Dutt, C. B. Poitras, and M. Lipson, "Overcoming Si_3N_4 film stress limitations for high quality factor ring resonators," Opt. Express **21**, 22829–22833 (2013).
39. Q. Li, A. A. Eftekhar, M. Sodagar, Z. Xia, A. H. Atabaki, and A. Adibi, "Vertical integration of high-*Q* silicon nitride microresonators into silicon-on-insulator platform," Opt. Express **21**, 18236–18248 (2013).
40. M. H. P. Pfeiffer, J. Liu, A. S. Raja, T. Morais, B. Ghadiani, and T. J. Kippenberg, "Ultra-smooth silicon nitride waveguides based on the Damascene reflow process: fabrication and loss origins," Optica **5**, 884–892 (2018).
41. H. El Dirani, L. Youssef, C. Petit-Etienne, S. Kerdiles, P. Grosse, C. Monat, E. Pargon, and C. Sciancalepore, "Ultralow-loss tightly confining Si_3N_4 waveguides and high-*Q* microresonators," Opt. Express **27**, 30726–30740 (2019).

42. Z. Ye, K. Twayana, P. A. Andrekson, and V. Torres-Company, "High-Q Si_3N_4 microresonators based on a subtractive processing for Kerr nonlinear optics," Opt. Express **27**, 35719–35727 (2019).
43. X. Ji, J. K. Jang, U. D. Dave, M. Corato-Zanarella, C. Joshi, A. L. Gaeta, and M. Lipson, "Exploiting ultralow loss multimode waveguides for broadband frequency combs," Laser Photon. Rev. **15**, 2000353 (2020).
44. J. Liu, G. Huang, R. N. Wang, J. He, A. S. Raja, T. Liu, N. J. Engelsen, and T. J. Kippenberg, "High-yield, wafer-scale fabrication of ultralow-loss, dispersion-engineered silicon nitride photonic circuits," Nat. Commun. **12**, 2236 (2021).
45. W. Jin, D. D. John, J. F. Bauters, T. Bosch, B. J. Thibeault, and J. E. Bowers, "Deuterated silicon dioxide for heterogeneous integration of ultra-low-loss waveguides," Opt. Lett. **45**, 3340–3343 (2020).
46. X. Ji, F. A. S. Barbosa, S. P. Roberts, A. Dutt, J. Cardenas, Y. Okawachi, A. Bryant, A. L. Gaeta, and M. Lipson, "Ultra-low-loss on-chip resonators with sub-milliwatt parametric oscillation threshold," Optica **4**, 619–624 (2017).
47. H. Zhou, Y. Geng, W. Cui, S. W. Huang, Q. Zhou, K. Qiu, and C. Wei Wong, "Soliton bursts and deterministic dissipative Kerr soliton generation in auxiliary-assisted microcavities," Light Sci. Appl. **8**, 1 (2019).
48. T. Herr, K. Hartinger, J. Riemensberger, C. Y. Wang, E. Gavartin, R. Holzwarth, M. L. Gorodetsky, and T. J. Kippenberg, "Universal formation dynamics and noise of Kerr-frequency combs in microresonators," Nat. Photonics **6**, 480–487 (2012).
49. M. Karpov, H. Guo, A. Kordts, V. Brasch, M. H. P. Pfeiffer, M. Zervas, M. Geiselmann, and T. J. Kippenberg, "Raman self-frequency shift of dissipative Kerr solitons in an optical microresonator," Phys. Rev. Lett. **116**, 103902 (2016).